Title

Aryl Diazonium-Assisted Amidoximation of MXene for Boosting Water Stability and Uranyl Sequestration via Electrochemical Sorption

Journal

ACS Applied Materials & Interfaces, 12(13)

ISSN

1944-8244

Authors

Zhang, Pengcheng

Wang, Lin

Huang, Zhiwei

et al.

Publication Date

2020-04-01

DOI

10.1021/acsami.0c00861

Peer reviewed

Aryl Diazonium-Assisted Amidoximation of MXene for Boosting Water Stability and Uranyl Sequestration via Electrochemical Sorption

Pengcheng Zhang,[#] Lin Wang,[#] Zhiwei Huang, Jipan Yu, Zijie Li, Hao Deng, Taiqi Yin, Liyong Yuan, John K. Gibson, Lei Mei, Lirong Zheng, Hongqing Wang, Zhifang Chai, and Weiqun Shi*

ABSTRACT: Despite that two-dimensional transition metal carbides and carbonitrides (MXenes) are burgeoning candidates for remediation of environmental pollutants, the construction of robust functionalized MXene nanosheets with a high affinity for target heavy metal ions and radionuclides remains a challenge. Here we report the successful placement of amidoxime chelating groups on $Ti_3C_2T_x$ MXene surface by diazonium salt grafting. The introduction of amidoxime functional groups significantly enhances the selectivity of $Ti_3C_2T_x$ nanosheets for uranyl ions and also greatly improves their stability in aqueous solution, enabling efficient, rapid, and recyclable uranium extraction from aqueous solutions containing competitive metal ions. Benefiting from the excellent conductivity of MXenes, the amidoxime functionalized $Ti_3C_2T_x$ nanosheets show outstanding electrochemical performance such that when loaded on carbon cloth the application of an electric field increases the uranium adsorption capacity from 294 to 626 mg/g, outperforming all organic electrochemical sorption materials reported previously. The present work provides an effective strategy to functionalize MXene nanosheets with fundamental implications for the design of MXene-based selective electrosorption electrode materials.

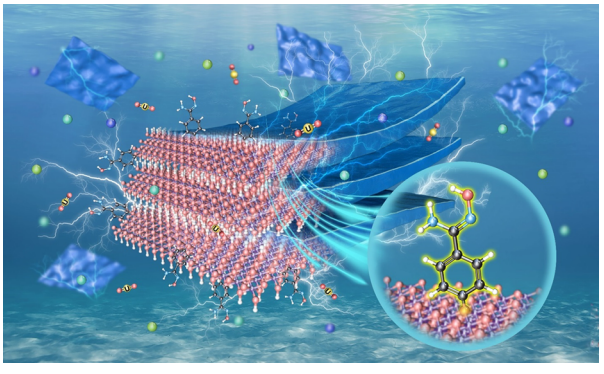

INTRODUCTION

Two-dimensional transition metal carbides and carbonitrides (MXenes) have garnered increasing attention in energy storage, environmental remediation, and interface catalysis due to properties of the unique layered structures such as metallic conductivity, high charge-carrier mobility, abundant active sorption sites, and versatile surface chemistry.[1−7] For environmental remediation, the properties of good hydrophilicity, controllable surface charge, and high redox activity render MXenes and their derivatives as promising adsorbents for pollutants such as dyes, heavy metal ions, radionuclides, and hazardous anionic species.[8] However, the deployment of MXene-based materials for complex environmental adsorption applications requires advances in stability control. Although exfoliation of multilayered MXene to yield super thin nanoflakes fully utilizes exposed active sites for sorption, such 2D MXenes are chemically unstable under most environmental conditions.[9,10] In particular, oxidation degradation of MXene nanosheets may results in undesirable rerelease of pollutants.

Another challenge in the deployment of inorganic MXene materials is the limited ion selectivity of the adsorbing surface hydroxyl groups but selective surface functional groups could ameliorate this shortcoming. However, in contrast to organic adsorbents, covalent grafting routes for MXene modification are rare,[11,12] mainly because relatively mild conditions are required to avoid the corrosion of MXene nanoflakes. Chemical grafting of aryl diazonium salts is a feasible and mild approach that conforms to principles of "green chemistry" and yields strong covalent bonds to the substrate surface.[13,14] Furthermore, this strategy can provide robust organic−inorganic hybrid materials,[15,16] which might enhance the stability of MXene nanosheets in aqueous solution.

As a central constituent of nuclear fuel cycles,[17] uranium is also a contaminant when released into the natural environment as highly mobile uranyl ions, denoted as U(VI).[18] The development of solid sorbents for U(VI) extraction offers

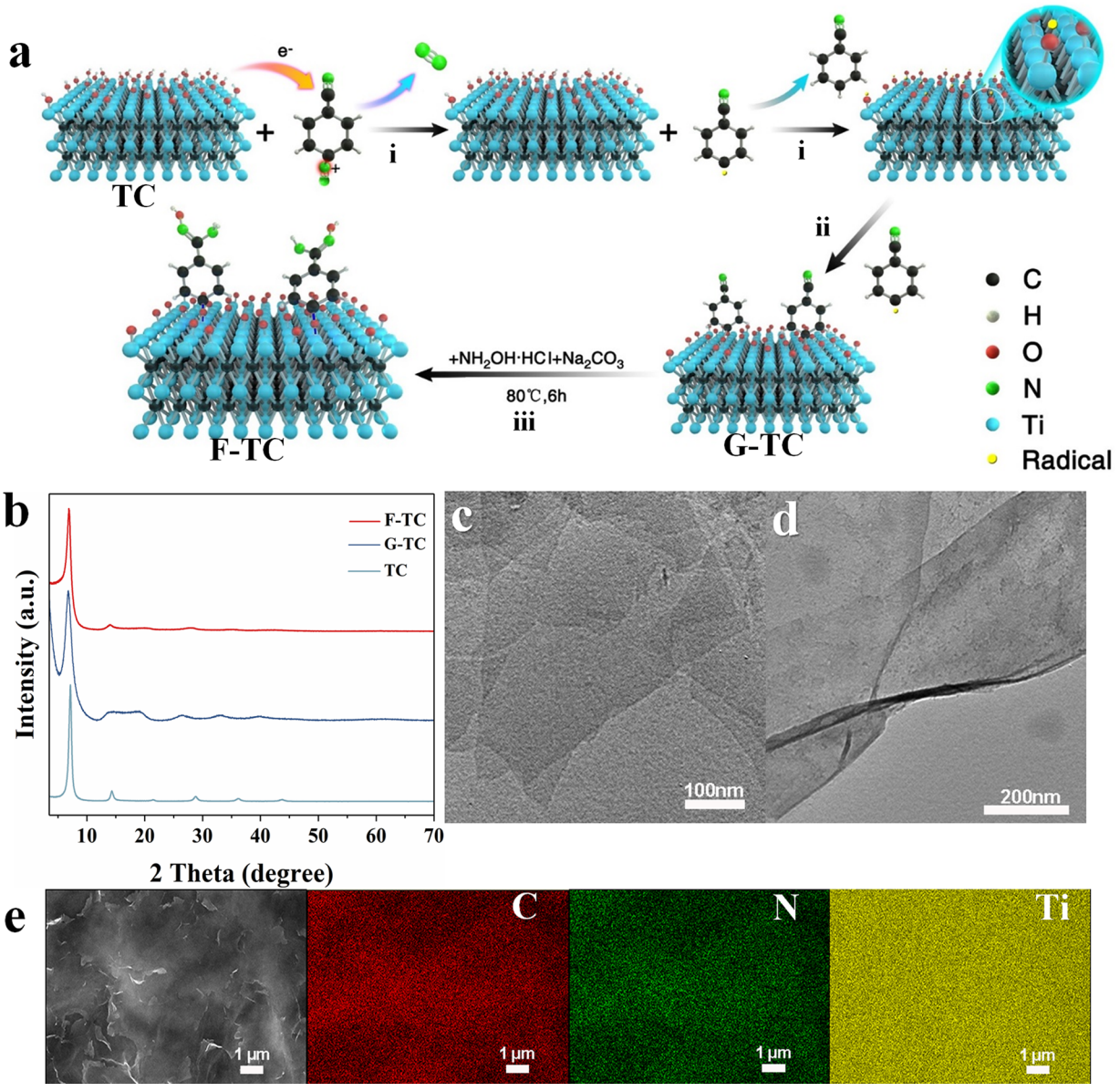

Figure 1. (a) Proposed mechanism for functionalization of $Ti_3C_2T_x$ MXene. (b) XRD patterns of TC, G-TC, and F-TC. TEM images of (c) TC and (d) F-TC. (e) SEM image (left) of F-TC and corresponding EDS elemental maps of C, N, and Ti.

opportunities to recycle uranium while reducing environmental contamination.[19] Although we previously demonstrated that MXenes could be used to remove U(VI) from the environment, selectivity for uranyl was limited.[20,21] Amidoxime has been demonstrated as a highly efficient uranyl capture functional group[22−29] with the nitrogen and oxygen atoms coordinating uranyl in a stable chelate structure. In the present work, we grafted amidoxime groups onto the surface of $Ti_3C_2T_x$ using diazonium salt to construct highly stable amidoxime functionalized MXene nanosheets (F-TC) with good selectivity for uranyl. Given the excellent conductivity of MXene,[30] electrosorption behavior of F-TC was assessed using the carbon cloth electrode. Upon application of a suitable alternating potential, the U(VI) capture capacity of F-TC more than doubles. To the best of our knowledge, this is the first demonstration of enhanced adsorption of environmental contaminants by electrosorption on MXene-based materials. The interaction mechanism between U(VI) and F-TC was elucidated by X-ray absorption and photoelectron spectroscopy.

EXPERIMENTAL SECTION

Synthesis of Multilayer Ti3C2Tx. Ti3AlC2 powders were purchased from Beijing Jinhezhi Materials Co., Ltd. A total of 3.75 g of Ti_3AlC_2 was slowly added to 100 mL of solution containing 9 M HCl and 6 g of LiF (Sinopharm Chemical Reagent Co., Ltd.). The mixture was stirred at 40 °C for 4 days, after which the product was centrifuged at 3500 rpm and washed three times each with 1 M HCl, 1 M LiCl, and deionized water.

Synthesis of $Ti_3C_2T_x$ Nanosheets (TC). $Ti_3C_2T_x$ nanosheets were obtained by ultrasonication and centrifugation with multilayer $Ti_3C_2T_x$. Ultrasonication was for 1 h, and centrifugation was for 30 min at 5000 rpm. The resulting supernatant was kept under inert gas.

Synthesis of Diazonium Salt Grafted $Ti_3C_2T_x$ Nanosheets (G-TC). 4-Cyanobenzenediazonium was synthesized as reported in the literature.[31] A solution of 4-aminobenzonitrile (Innochem (Beijing) Technology Co., Ltd.) (1.9 g) in acetic acid (7.5 mL) was added to 16 mL of concentrated HCl. Then $NaNO_2$ (1.335 g) in 5 mL of H_2O

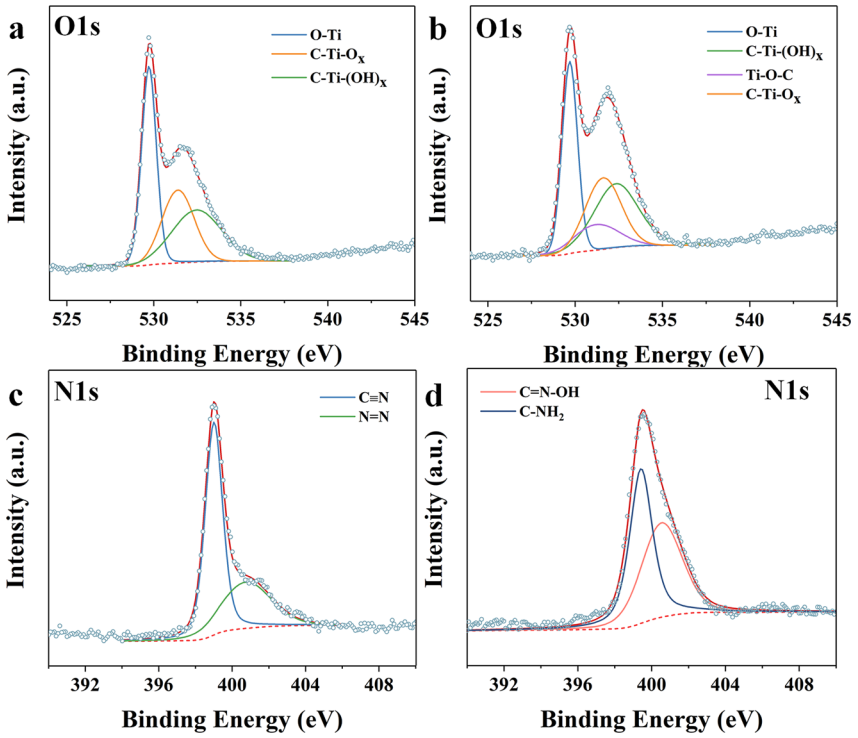

Figure 2. XPS spectra of $Ti_3C_2T_x$ nanoflakes before and after grafting. High-resolution O 1s region of (a) TC and (b) G-TC and N 1s region of (c) G-TC and (d) F-TC.

was added dropwise to this solution after cooling to 0 °C. After 30 min, this prepared solution was dripped into the precooled TC aqueous solution (600 mg) (the concentration of TC aqueous solution is between 13 and 15 mg/mL) and kept stirred at 1500 rpm for 6 h (ensuring that there is not a lot of bubble agglomeration on the surface of the solution). After the reaction time, the solution was sonicated for 15 min and centrifuged at 10 000 rpm for 30 min; then the upper liquid was poured and washed successively by water, acetone, and ethanol in order to remove salts (5 min each time, 10 000 rpm).

Preparation of Amidoxime-Functionalized $Ti_3C_2T_x$ Nanosheets (F-TC). The obtained G-TC (90 mg) was treated with Na_2CO_3 (255 mg) and $NH_2OH{\cdot}HCl$ (334.5 mg) in a H_2O(3.6 mL)/C_2H_5OH(30 mL) solution for 6 h at 80 °C in a reactor (Teflon-lined autoclave) of 50 mL. The product was rinsed with DI water and ethanol.[32]

Electrode Preparation. F-TC_CC: The F-TC was uniformly dispersed in water, and ethanol was added to $V_{ethanol}/V_{water}$ = 3:1, followed by the addition of naphthol (Alfa Aesar) to yield $V_{ethanol+water}/V_{naphthol}$ = 50:1. The solution was then dripped onto the surface of carbon cloth (HCP331N, Shanghai Hesen Electric Co., Ltd.) and dried at room temperature in air.

PAO_CC: PAO was prepared according to literature reports,[33] then dripped onto the surface of carbon cloth and dried at room temperature in air.

The quality control of F-TC and PAO is around 2.3 mg.

Batch Sorption Experiments. $UO_2(NO_3)_2{\cdot}6H_2O$ (Sinopharm Chemical Reagent Co. Ltd.) was dissolved in deionized water to prepare a 200 mg/L U(VI) stock solution. A series of U(VI) sorption experiments using F-TC samples at 25 °C under air conditions were carried out as a function of pH, contact time, and initial U(VI) concentration. After F-TC was mixed with deionized water, NaCl, and the desired amount of U(VI), the pH was adjusted using 0.1 M NaOH and 0.1 M HCl. The solid extractant was separated after 7 h by centrifuging at 10 000 rpm for 10 min for characterization. The supernatants were collected using poly(ether sulfone) syringe filters (0.22 μm, ANPEL Scientific Instrument Co., Ltd., Shanghai) and diluted with 5 wt % HNO_3 before determination of uranium concentration. The removal capacity Q_e (mg/g) was calculated as $Q_e = (C_0 - C_e)V/m$, where C_0 and C_e are initial and final concentrations of cations, and V and m are the solution volume and the mass of solid sorbent. With noted exceptions, the conditions were $m_{sorbent}/V_{solution}$ = 0.2 mg/mL, pH 5.0, air atmosphere.

Electrosorption Experiments. All electrosorption experiments were carried out under a three-electrode system: Ag/AgCl as a reference electrode, and platinum wire as a counter electrode. Electrosorption was performed in an air atmosphere with a stirring rate of 200 rpm. The volume of the solution was 50 mL. The initial pH was 5.0. In order to test the concentration of uranyl ions at different times, the volume of each sample is 200 μL.

RESULTS AND DISCUSSION

$Ti_3C_2T_x$ nanosheets (TC) were prepared by a typical ultrasound exfoliation of LiF-HCl etched multilayer $Ti_3C_2T_x$.[34] The disappearance of nonbasal directions X-ray diffraction (XRD) peaks (around 61°) (Figure S1) and morphology changes after exfoliation (Figure S2a,b) indicate successful conversion of the multilayer material to a few-layer MXene material.[35] Figure 1a shows the proposed mechanism for grafting amidoxime onto the surface of MXene. Providing an electron to the aryl diazonium results in the cleavage of diazonium with nitrogen release and the production of a free radical (i), which substitutes onto the MXene surface of substrate to form a strong Ti—O—C covalent bond (ii). Finally, F-TC is synthesized by reacting hydroxylamine with surface cyano groups on diazonium grafted MXene (G-TC) under mild alkali-assisted hydrothermal conditions (iii). The XRD patterns in Figure 1b show that the (002) peaks of G-TC and F-TC around 7° exhibit a small shift to lower angles compared with TC, indicative of the functionalized groups on the surface and/or edges of MXene nanoflakes. Examination of surface morphologies of the TC, G-TC, and F-TC (Figure 1c,d, Figure S2) by transmission and scanning electron

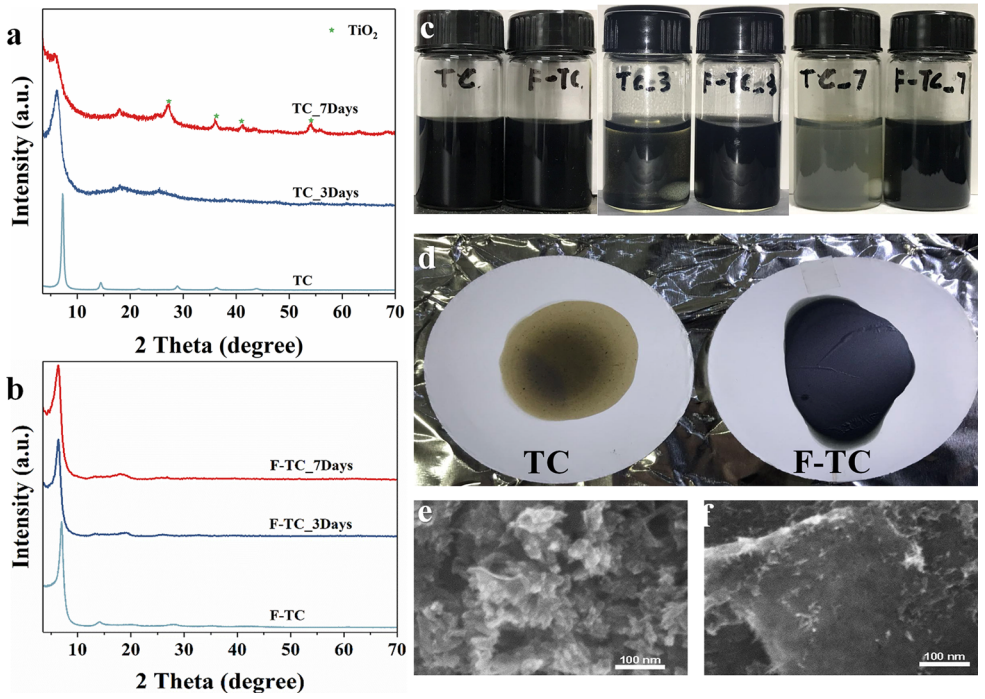

Figure 3. XRD patterns of (a) TC and (b) F-TC before and after immersion in water under air atmosphere for 0 days (TC), 3 days (TC_3), and 7 days (TC_7). Photos of (c) dispersed aqueous solutions after the different immersion durations, and (d) filtered samples of TC and F-TC after immersion in water. SEM images of (e) TC and (f) F-TC after 14 days of immersion in water. All results are for concentration of 0.1 mg/mL and at room temperature.

microscopy (TEM and SEM) reveals that modified MXenes G-TC and F-TC retain the uniform slice structure of TC, though the surfaces and edges become less regular upon functionalization. Atomic force microscopy (AFM) revealed that the thickness of MXene flakes increases by about 0.8 nm upon amidoxime grafting (Figure S3).

Chemical species on MXene surface before and after modification were assessed by several techniques. Fourier transform infrared (FTIR) spectroscopy confirmed formation of a cyano group, followed by conversion to amidoxime on the TC surface (Figure S4). In particular, the IR band at 2212 cm^{-1} for G-TC corresponds to the surface cyano C≡N stretch mode.[36] After 6 h of treatment with hydroxylamine hydrochloride, a new IR peak appeared at 1649 cm^{-1}, which is assigned to the stretch mode of amidoxime C═N on F-TC.[37,38] Thermogravimetric analysis (TGA) revealed the weight percent of functional groups to be about 20.2% for G-TC and 19.6% for F-TC (Figure S5). Energy dispersive X-ray spectroscopy (EDS) results in Figure 1e indicate the homogeneous distribution of amidoxime functional groups on F-TC. High-resolution X-ray photoelectron spectra (XPS) of TC, G-TC, and F-TC after modification are shown in Figure 2. For the O 1s region, peaks at 532.45, 531.39, and 529.72 eV correspond respectively to C−Ti−$(OH)_x$, C−Ti−O_x, and Ti−O linkages on the surface of TC.[39] Comparison of Figure 2, panels a and b, reveals a new O 1s peak at 531.2 eV after diazonium grafting, which is due to the formed Ti−O−C linkages.[40] Fitting of the N 1s peaks around 400 eV for G-TC reveals C≡N and N═N bonds with features at 399.0 and 400.8 eV, respectively.[41,42] Upon hydrothermal treatment, the N 1s spectrum reveals C═N−OH and C−NH_2 linkages of F-TC at 400.5 and 399.45 eV, respectively, confirming synthesis of amidoxime functionalized MXene.[43]

Stability of MXene nanosheet materials is critical to their performance in real-world applications.[44] To assess the stability of $Ti_3C_2T_x$ nanosheets before and after modification, TC and F-TC were dispersed in aqueous solution and exposed to the air for different time periods. After 7 days of treatment, XRD of TC revealed substantial broadening of the (002) peak, and partial oxidation of MXene to TiO_2 (Figure 3a and Figure S6).[44−46] Negligible changes in the corresponding XRD patterns for treated F-TC (Figure 3b) demonstrated significant stabilization toward oxidation and degradation. The corresponding optical photos in Figure 3c,d confirm that the treated F-TC retained good colloidal dispersion with retention of the original black color whereas the treated TC was degraded. The enhanced oxidation resistance of modified MXene was further confirmed by SEM (Figure 3e,f): oxide nanoparticles are apparent in TC that correspond to TiO_2 as identified in Figure 3a, whereas the slice structures of F-TC were maintained after exposure to air and water. It has been reported that the edges of MXene nanosheets are highly reactive and thus preferentially degrade in aqueous solution.[47] Moreover, the presence of surface defects on MXene nanosheets may also lead to the structural instability. High-resolution TEM images in Figure S7 have clearly shown that the roughness of MXene edges and surfaces changes after the functionalization. Consequently, we propose that the active edge and surface sites of TC bond with diazonium free radicals during grafting with the protection afforded by the functional groups thereby enhancing the stability of the organic−inorganic hybrid F-TC MXene, which facilitates the utility for removal of contaminants from water. Recyclability, an important criterion for practical applications of solid adsorbents, has been rarely reported for MXene nanoflake materials because of their instability. As discussed below, the relatively high stability of F-TC will allow recyclability in environmental cleanup applications.

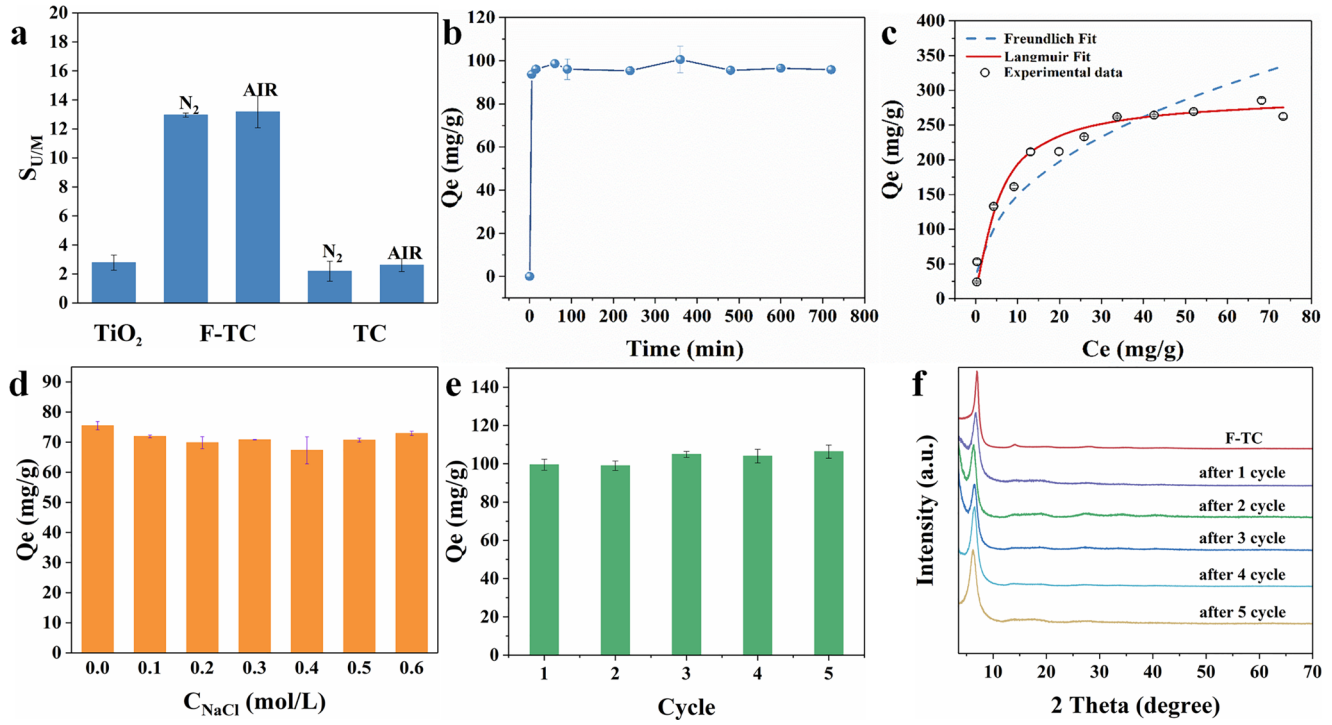

Figure 4. (a) U/Eu separation factor of TiO_2, F-TC, and TC from a competitive adsorption solution containing U(VI) and Eu(III). (b–d) U(VI) adsorption onto F-TC as a function of contact time (b), equilibrium concentration (c), and ionic strength (d). (e) Reusability of FTC for U(VI) adsorption. (f) The corresponding XRD patterns of F-TC after each reuse cycle. Initial concentrations: (a) [U] = [Eu] = 50 ppm, (b) [U] = 21 ppm, (d) [U] = 16 ppm, (e) [U] = 20 ppm.

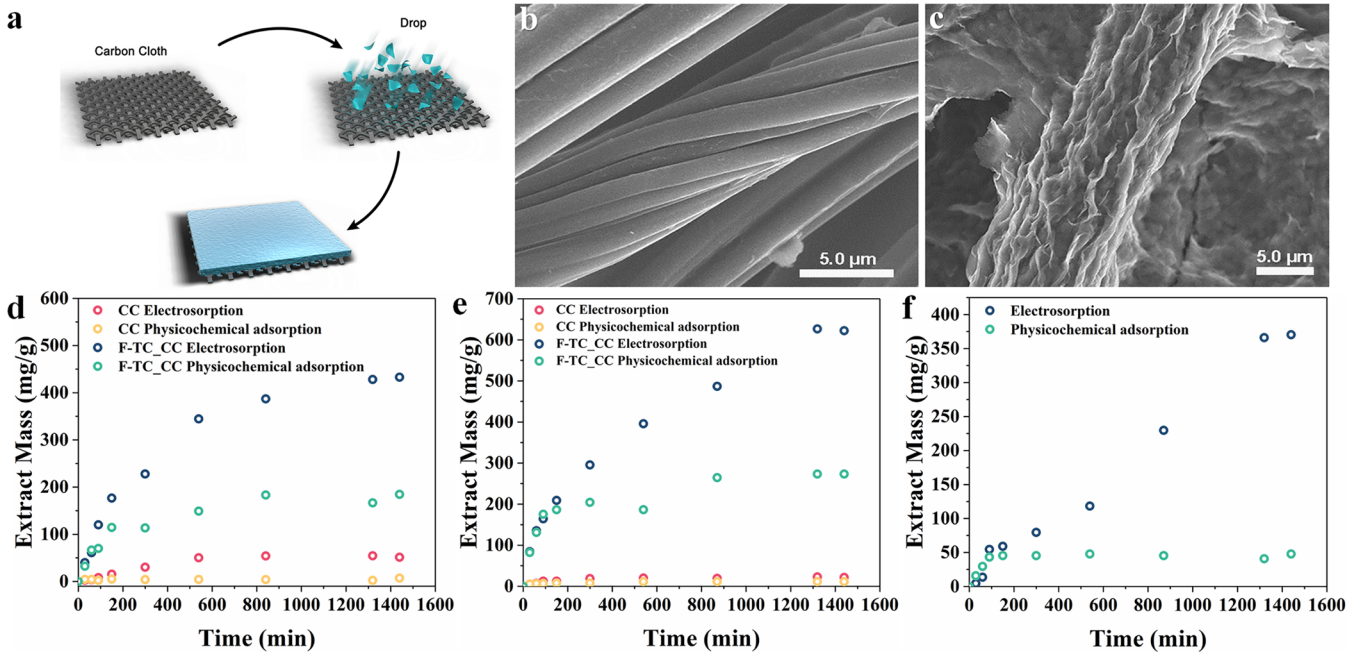

Figure 5. (a) Schematic for preparation of composite F-TC_CC electrode. SEM images of (b) pristine CC and (c) modified F-TC_CC electrode. (d) Electrosorption performance of pristine CC and F-TC_CC electrodes for U(VI) removal in potentiostatic mode. (e) Electrosorption performance in alternating potential (AP) mode. (f) Electrosorption performance of PAO under the same AP conditions as in (e). Initial concentration of uranium: (d) 20, (e) 50, and (f) 50 ppm.

Competitive adsorption experiments were conducted to investigate the selectivity of F-TC for uranyl with Eu(III) selected as a representative trivalent lanthanide since typical inorganic and organic–inorganic hybrid sorbents typically have poor selectivity for U(VI) versus Eu(III).[48−50] Results in Figure 4a show that F-TC can separate U(VI) from Eu(III) efficiently with a separation factor ($S_{U/Eu}$) of about 13, which is significantly higher than $S_{U/M}$ of TiO_2 and pristine TC. The lower uranyl selectivity of TC versus F-TC presumably reflects that terminating hydroxyl groups of TC exhibit poor metal ion

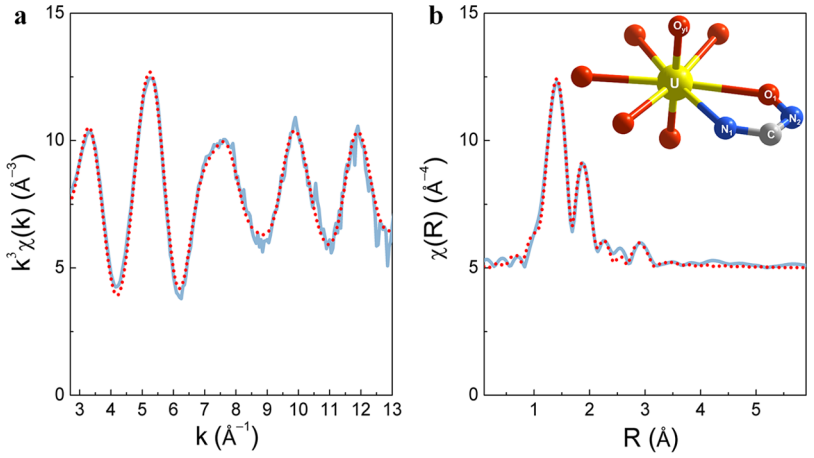

Figure 6. (a) U L_3 edge k^3-weighted EXAFS spectra (solid lines) and the best theoretical fits (dotted lines) of U-loaded F-TC sample at pH 5.0. (b) Corresponding nonphase shift corrected Fourier transforms. The proposed coordination is shown in (b).

discrimination.[51] The present results demonstrate that amidoxime modification of a MXene surface greatly enhances selective adsorption of uranyl ions. The corresponding distribution coefficient (K_d) for U(VI) was calculated as $>10^4$ from Eu/U competitive adsorption experiments, such that F-TC should effectively extract U(VI) from wastewater containing competing ions.[52−54] The selectivity of F-TC is similar for both air or nitrogen atmospheres (Figure 4a) in accordance with the demonstrated resistance to degradation by oxidation.

The kinetic data for U(VI) sorption on F-TC in Figure 4b show that more than 95% of uranyl is removed after 5 min at pH 5.0. Such fast kinetics reflect the excellent hydrophilicity and fully exposed adsorption sites of F-TC. The sorption isotherm in Figure 4c is well-fitted by the Langmuir model (Figure S8 and Table S1), indicating heterogeneous monolayer adsorption of U(VI) on F-TC.[55,56] The saturated U(VI) adsorption capacity, determined as 294 mg/g, is greater than most inorganic sorbents or modified hybrid materials based on silicon and carbon (Table S2). Figure 4d demonstrates the ability of F-TC to capture U(VI) under high salinity up to ∼0.6 M NaCl. Such ionic strength-independent sorption behavior suggests the stable inner-sphere surface complexation of U(VI) by amidoxime functionalized MXene.[57,58] The recyclability of F-TC for U(VI) extraction was assessed using 0.1 M Na_2CO_3 as an eluent with the results shown in Figure 4e,f. It is evident that F-TC can be fully regenerated for at least five sorption/desorption cycles (Figure 4e) with preservation of the F-TC nanosheet structure as evidenced by the invariant (002) XRD peak (Figure 4f). The results summarized in Figure 4 suggest F-TC as an efficient and robust MXene-based material for rapid and selective uranium extraction from aqueous solutions. The more general applicability of diazonium salt modification for MXene functionalization was further demonstrated by grafting carboxyl groups onto $Ti_3C_2T_x$ nanosheets (Figure S9). Like F-TC, the carboxyl functionalized TC exhibited excellent sorption capacity, >300 mg/g, for U(VI) removal.

Given the excellent conductivity of MXene, electrosorption was evaluated for F-TC loaded onto carbon cloth electrode (F-TC_CC) for comparison with sorption by unloaded carbon cloth electrode (CC) (Figure 5a−c). Applying a constant negative bias voltage (−0.7 V) to the F-TC modified electrode generates an electric field to promote migration and enrichment of uranyl ions at the cathode, which results in higher U(VI) removal capacity for electrosorption versus physicochemical adsorption (Figure 5d). However, potentiostatic electrosorption usually introduces a capacitive deionization (CDI) contribution,[59−61] which is disadvantageous for selective ion extraction even though the total ion adsorption increases. In accord with a CDI contribution, the results for the unloaded carbon cloth (CC) in Figure 5d indicate considerable electrosorption enhancement. To overcome the CDI effect, a periodic alternating potential (AP) method was adopted, in which the bias voltage for selective capture of U(VI) was applied in the first half of the AP period (−0.7 V, 1 s), whereas in the second half removal of thebias voltage released adsorbed ions which were not sequestered by functional groups (Figure S10).[33] The AP method prevents competing ions from blocking active chelation sites and eliminates nonspecific adsorption of uranium on unmodified substrate with a result that the U(VI) extraction capacity on F-TC modified electrode reached up to 626 mg/g. This U(VI) removal capacity is apparently larger than the electrosorption performance of traditional materials such as graphene and activated carbon (Table S2). The AP results furthermore show that CDI adsorption of U(VI) is minimal on carbon cloth (Figure 5e). The results summarized in Figure 5 demonstrate selective electrosorption for uranium extraction using an AP approach.

The organic polyamidoxime (PAO) terminated with the same functional groups as F-TC was synthesized for the assessment of its electrosorption performance. Since the charge transfer in PAO is poor, carbon black was used to enhance conductivity. Physicochemical adsorption of U(VI) on PAO is low (<50 mg/g; Figure 5f), possibly due to low surface exposure of chelating sites. Upon application of the same AP as used for F-TC_CC (Figure 5e), the extracted mass of U(VI) per unit PAO is significantly enhanced but is still only ∼60% of the value achieved with F-TC after 12 h electrosorption (Figure 5f). Treatment of uranium-contaminated simulated groundwater (Table S3) by F-TC and PAO was performed to assess electrosorption in complex aqueous environments. Here, a more negative potential and a much higher-frequency AP period were adopted to maximize uranium removal while avoiding water splitting.[33] As shown in Figure S11, uranium extraction by F-TC reaches ∼230 mg/g, which is about 40% higher than that of PAO.

The coordination environment of extracted uranium on F-TC was investigated by XPS and synchrotron radiation extended X-ray absorption fine structure (EXAFS) spectroscopy. The characteristic U 4f signal is apparent in XPS survey scans for F-TC after uranyl adsorption (Figure S12). The high-resolution XPS spectrum in Figure S13 shows that the N 1s binding energy peak increases by 0.5 eV upon uranium sequestration, suggesting that the amidoxime N atom directly participates in U(VI) coordination. Figure 6 shows the measured and fitted U L_3 edge k^3-weighted EXAFS spectrum and its Fourier transform with the resulting fitting parameters such as coordination number and bond distance summarized in Table S4. In addition to the typical axial distance for uranyl O_{yl} atoms (U—O_{yl} ≈ 1.80 Å) and equatorial distance for coordinated water O_w atoms (U—O_w ≈ 2.36 Å), about two atoms at 2.55 Å in the first coordination shell of U are ascribed to the O atom of oximido and the amino N atom of the amidoxime group (U—O_1/N_1, inset of Figure 6b); another two atoms at 3.41 Å are assigned as the adjacent N and C atoms (U—N_2/C). These U—O_1/N_1 and U—N_2/C distances are consistent with those reported by Tian et al. for a uranium compound with a small tridentate-binding molecule.[62] The EXAFS fitting results suggest that the uranyl coordinates with F-TC amidoxime groups to form 1:1 bidentate chelating complexes (inset of Figure 6b). Although this bidentate chelating configuration has not yet been reported in a crystal structure, recent experimental studies and modeling of cooperative chelating by Abney et al. support this coordination.[63]

CONCLUSION

In summary, we reported for the first time the introduction of amidoxime functional groups onto the surface of MXene using diazonium. The soft chemical grafting method provides a Ti—O—C covalent bond between benzonitrile and MXene substrate, which allows for subsequent in situ conversion to terminating amidoxime groups. The successful modification by amidoxime increases the oxidation resistance of MXene in aqueous solution, and significantly improves the selective chelation of uranyl for environmental remediation. The use of a periodic alternating potential on a F-TC modified electrode further enhances the extraction capacity while maintaining selectivity for uranyl. F-TC exhibits superior electrosorption performance compared with previously reported amidoxime functionalized organic materials. The results demonstrate amidoxime functionalized MXene as a new platform for rapid, efficient, and selective extraction of uranium from complex aqueous solutions.

ASSOCIATED CONTENT

Supporting Information

The Supporting Information is available free of charge at https://pubs.acs.org/doi/10.1021/acsami.0c00861.

Details of functional group graft ratio calculation; sorption data fitting models; XRD of MAX phase, multilayer $Ti_3C_2T_X$, TC_7 Days, and carboxyl functionalized TC; SEM of multilayer $Ti_3C_2T_X$, TC, G-TC, and F-TC; AFM of TC and F-TC; FTIR data of TC, G-TC, F-TC, and carboxyl functionalized TC; TGA curves of TC, G-TC, and F-TC; XPS data of F-TC and F-TC_U; electrosorption of F-TC and PAO in groundwater samples; EXAFS fitting parameters (PDF)

Corresponding Author

Weiqun Shi − *Laboratory of Nuclear Energy Chemistry, Institute of High Energy Physics, Chinese Academy of Sciences, Beijing 100049, China;* orcid.org/0000-0001-9929-9732; Email: shiwq@ihep.ac.cn

Authors

Pengcheng Zhang − *Laboratory of Nuclear Energy Chemistry, Institute of High Energy Physics, Chinese Academy of Sciences, Beijing 100049, China; School of Chemistry and Chemical Engineering, University of South China, Hengyang 421001, China*

Lin Wang − *Laboratory of Nuclear Energy Chemistry, Institute of High Energy Physics, Chinese Academy of Sciences, Beijing 100049, China;* orcid.org/0000-0002-1539-9865

Zhiwei Huang − *Laboratory of Nuclear Energy Chemistry, Institute of High Energy Physics, Chinese Academy of Sciences, Beijing 100049, China;* orcid.org/0000-0003-2660-3136

Jipan Yu − *Laboratory of Nuclear Energy Chemistry, Institute of High Energy Physics, Chinese Academy of Sciences, Beijing 100049, China*

Zijie Li − *Laboratory of Nuclear Energy Chemistry, Institute of High Energy Physics, Chinese Academy of Sciences, Beijing 100049, China*

Hao Deng − *Laboratory of Nuclear Energy Chemistry, Institute of High Energy Physics, Chinese Academy of Sciences, Beijing 100049, China*

Taiqi Yin − *Laboratory of Nuclear Energy Chemistry, Institute of High Energy Physics, Chinese Academy of Sciences, Beijing 100049, China*

Liyong Yuan − *Laboratory of Nuclear Energy Chemistry, Institute of High Energy Physics, Chinese Academy of Sciences, Beijing 100049, China;* orcid.org/0000-0003-4261-8717

John K. Gibson − *Chemical Sciences Division, Lawrence Berkeley National Laboratory, Berkeley 94720, United States;* orcid.org/0000-0003-2107-5418

Lei Mei − *Laboratory of Nuclear Energy Chemistry, Institute of High Energy Physics, Chinese Academy of Sciences, Beijing 100049, China;* orcid.org/0000-0002-2926-7265

Lirong Zheng − *Beijing Synchrotron Radiation Facility, Institute of High Energy Physics, Chinese Academy of Sciences, Beijing 100049, China*

Hongqing Wang − *School of Chemistry and Chemical Engineering, University of South China, Hengyang 421001, China*

Zhifang Chai − *Engineering Laboratory of Advanced Energy Materials, Ningbo Institute of Industrial Technology, Chinese Academy of Sciences, Ningbo 315201, China*

Author Contributions

# P.Z. and L.W. contributed equally.

Notes

The authors declare no competing financial interest.

ACKNOWLEDGMENTS

This work was supported by the Natural Science Foundation of China (Grants 11675192, 21836001, 21777161, 11975016, and 21577144) and the National Science Fund for Distinguished Young Scholars (Grant 21925603). The Science

Challenge Project (TZ2016004) is also acknowledged. We are grateful to the staff of Beijing Synchrotron Radiation Facility (BSRF) for EXAFS and XANES measurement.

REFERENCES

(1) Wang, X.; Mathis, T. S.; Li, K.; Lin, Z.; Vlcek, L.; Torita, T.; Osti, N. C.; Hatter, C.; Urbankowski, P.; Sarycheva, A.; Tyagi, M.; Mamontov, E.; Simon, P.; Gogotsi, Y. Influences from solvents on charge storage in titanium carbide MXenes. *Nat. Energy* **2019**, *4*, 241−248.

(2) Xie, X.; Chen, C.; Zhang, N.; Tang, Z.-R.; Jiang, J.; Xu, Y.-J. Microstructure and surface control of MXene films for water purification. *Nat. Sustain.* **2019**, *2*, 856−862.

(3) Persson, I.; Halim, J.; Lind, H.; Hansen, T. W.; Wagner, J. B.; Naslund, L. A.; Darakchieva, V.; Palisaitis, J.; Rosen, J.; Persson, P. O. A. 2D Transition Metal Carbides (MXenes) for Carbon Capture. *Adv. Mater.* **2019**, *31*, 1805472.

(4) Peng, Q.; Guo, J.; Zhang, Q.; Xiang, J.; Liu, B.; Zhou, A.; Liu, R.; Tian, Y. Unique lead adsorption behavior of activated hydroxyl group in two-dimensional titanium carbide. *J. Am. Chem. Soc.* **2014**, *136*, 4113−4116.

(5) Anasori, B.; Lukatskaya, M. R.; Gogotsi, Y. 2D metal carbides and nitrides (MXenes) for energy storage. *Nat. Rev. Mater.* **2017**, *2*, 16098−160114.

(6) Er, D.; Li, J.; Naguib, M.; Gogotsi, Y.; Shenoy, V. B. Ti(3)C(2) MXene as a high capacity electrode material for metal (Li, Na, K, Ca) ion batteries. *ACS Appl. Mater. Interfaces* **2014**, *6*, 11173−11179.

(7) Yun, J.; Echols, I.; Flouda, P.; Wang, S.; Easley, A.; Zhao, X.; Tan, Z.; Prehn, E.; Zi, G.; Radovic, M.; Green, M. J.; Lutkenhaus, J. L. Layer-by-Layer Assembly of Polyaniline Nanofibers and MXene Thin-Film Electrodes for Electrochemical Energy Storage. *ACS Appl. Mater. Interfaces* **2019**, *11*, 47929−47938.

(8) Zhang, Q.; Teng, J.; Zou, G.; Peng, Q.; Du, Q.; Jiao, T.; Xiang, J. Efficient phosphate sequestration for water purification by unique sandwich-like MXene/magnetic iron oxide nanocomposites. *Nanoscale* **2016**, *8*, 7085−7093.

(9) Zhao, X.; Vashisth, A.; Prehn, E.; Sun, W.; Shah, S. A.; Habib, T.; Chen, Y.; Tan, Z.; Lutkenhaus, J. L.; Radovic, M.; Green, M. J. Antioxidants Unlock Shelf-Stable Ti3C2T (MXene) Nanosheet Dispersions. *Matter* **2019**, *1*, 513−526.

(10) Zhang, C. J.; Pinilla, S.; McEvoy, N.; Cullen, C. P.; Anasori, B.; Long, E.; Park, S.-H.; Seral-Ascaso, A.; Shmeliov, A.; Krishnan, D.; Morant, C.; Liu, X.; Duesberg, G. S.; Gogotsi, Y.; Nicolosi, V. Oxidation Stability of Colloidal Two-Dimensional Titanium Carbides (MXenes). *Chem. Mater.* **2017**, *29*, 4848−4856.

(11) Zhang, S.; Liu, H.; Cao, B.; Zhu, Q.; Zhang, P.; Zhang, X.; Chen, R.; Wu, F.; Xu, B. An MXene/CNTs@P nanohybrid with stable Ti−O−P bonds for enhanced lithium ion storage. *J. Mater. Chem. A* **2019**, *7*, 21766−21773.

(12) Wang, H.; Zhang, J.; Wu, Y.; Huang, H.; Li, G.; Zhang, X.; Wang, Z. Surface modified MXene Ti 3 C 2 multilayers by aryl diazonium salts leading to large-scale delamination. *Appl. Surf. Sci.* **2016**, *384*, 287−293.

(13) Mahouche-Chergui, S.; Gam-Derouich, S.; Mangeney, C.; Chehimi, M. M. Aryl diazonium salts: a new class of coupling agents for bonding polymers, biomacromolecules and nanoparticles to surfaces. *Chem. Soc. Rev.* **2011**, *40*, 4143−4166.

(14) Martin, C.; Alias, M.; Christien, F.; Crosnier, O.; Bélanger, D.; Brousse, T. Graphite-Grafted Silicon Nanocomposite as a Negative Electrode for Lithium-Ion Batteries. *Adv. Mater.* **2009**, *21*, 4735−4741.

(15) Belanger, D.; Pinson, J. Electrografting: a powerful method for surface modification. *Chem. Soc. Rev.* **2011**, *40*, 3995−4048.

(16) Ryder, C. R.; Wood, J. D.; Wells, S. A.; Yang, Y.; Jariwala, D.; Marks, T. J.; Schatz, G. C.; Hersam, M. C. Covalent functionalization and passivation of exfoliated black phosphorus via aryl diazonium chemistry. *Nat. Chem.* **2016**, *8*, 597−602.

(17) Ivanov, A. S.; Parker, B. F.; Zhang, Z.; Aguila, B.; Sun, Q.; Ma, S.; Jansone-Popova, S.; Arnold, J.; Mayes, R. T.; Dai, S.; Bryantsev, V. S.; Rao, L.; Popovs, I. Siderophore-inspired chelator hijacks uranium from aqueous medium. *Nat. Commun.* **2019**, *10*, 819−825.

(18) Chu, S.; Majumdar, A. Opportunities and challenges for a sustainable energy future. *Nature* **2012**, *488*, 294−303.

(19) Yu, J.; Yuan, L.; Wang, S.; Lan, J.; Zheng, L.; Xu, C.; Chen, J.; Wang, L.; Huang, Z.; Tao, W.; Liu, Z.; Chai, Z.; Gibson, J. K.; Shi, W. Phosphonate-Decorated Covalent Organic Frameworks for Actinide Extraction: A Breakthrough Under Highly Acidic Conditions. *CCS Chem.* **2019**, *1*, 286−295.

(20) Wang, L.; Tao, W.; Yuan, L.; Liu, Z.; Huang, Q.; Chai, Z.; Gibson, J. K.; Shi, W. Rational control of the interlayer space inside two-dimensional titanium carbides for highly efficient uranium removal and imprisonment. *Chem. Commun.* **2017**, *53*, 12084−12087.

(21) Wang, L.; Song, H.; Yuan, L.; Li, Z.; Zhang, Y.; Gibson, J. K.; Zheng, L.; Chai, Z.; Shi, W. Efficient U(VI) Reduction and Sequestration by Ti2CT x MXene. *Environ. Sci. Technol.* **2018**, *52*, 10748−10756.

(22) Abney, C. W.; Mayes, R. T.; Saito, T.; Dai, S. Materials for the Recovery of Uranium from Seawater. *Chem. Rev.* **2017**, *117*, 13935−14013.

(23) Sun, Q.; Aguila, B.; Earl, L. D.; Abney, C. W.; Wojtas, L.; Thallapally, P. K.; Ma, S. Covalent Organic Frameworks as a Decorating Platform for Utilization and Affinity Enhancement of Chelating Sites for Radionuclide Sequestration. *Adv. Mater.* **2018**, *30*, 1705479.

(24) Sun, Y.; Lu, S.; Wang, X.; Xu, C.; Li, J.; Chen, C.; Chen, J.; Hayat, T.; Alsaedi, A.; Alharbi, N. S.; Wang, X. Plasma-Facilitated Synthesis of Amidoxime/Carbon Nanofiber Hybrids for Effective Enrichment of 238U(VI) and 241Am(III). *Environ. Sci. Technol.* **2017**, *51*, 12274−12282.

(25) Sun, Q.; Aguila, B.; Perman, J.; Ivanov, A. S.; Bryantsev, V. S.; Earl, L. D.; Abney, C. W.; Wojtas, L.; Ma, S. Bio-inspired nano-traps for uranium extraction from seawater and recovery from nuclear waste. *Nat. Commun.* **2018**, *9*, 1644−1652.

(26) Zhang, L.; Pu, N.; Yu, B.; Ye, G.; Chen, J.; Xu, S.; Ma, S. Skeleton Engineering of Homocoupled Conjugated Microporous Polymers for Highly Efficient Uranium Capture via Synergistic Coordination. *ACS Appl. Mater. Interfaces* **2020**, *12*, 3688−3696.

(27) Li, B.; Sun, Q.; Zhang, Y.; Abney, C. W.; Aguila, B.; Lin, W.; Ma, S. Functionalized porous aromatic framework for efficient uranium adsorption from aqueous solutions. *ACS Appl. Mater. Interfaces* **2017**, *9*, 12511−12517.

(28) Aguila, B.; Sun, Q.; Cassady, H.; Abney, C. W.; Li, B.; Ma, S. Design Strategies to Enhance Amidoxime Chelators for Uranium Recovery. *ACS Appl. Mater. Interfaces* **2019**, *11*, 30919−30926.

(29) Sun, Q.; Aguila, B.; Ma, S. Opportunities of porous organic polymers for radionuclide sequestration. *Trends in Chemistry* **2019**, *1*, 292−303.

(30) VahidMohammadi, A.; Mojtabavi, M.; Caffrey, N. M.; Wanunu, M.; Beidaghi, M. Assembling 2D MXenes into Highly Stable Pseudocapacitive Electrodes with High Power and Energy Densities. *Adv. Mater.* **2019**, *31*, 1806931.

(31) Gallagher, N. M.; Bauer, J. J.; Pink, M.; Rajca, S.; Rajca, A. High-Spin Organic Diradical with Robust Stability. *J. Am. Chem. Soc.* **2016**, *138*, 9377−9380.

(32) Zhao, Y.; Wang, X.; Li, J.; Wang, X. Amidoxime functionalization of mesoporous silica and its high removal of U(vi). *Polym. Chem.* **2015**, *6*, 5376−5384.

(33) Liu, C.; Hsu, P.-C.; Xie, J.; Zhao, J.; Wu, T.; Wang, H.; Liu, W.; Zhang, J.; Chu, S.; Cui, Y. A half-wave rectified alternating current electrochemical method for uranium extraction from seawater. *Nat. Energy* **2017**, *2*, 17007−17014.

(34) Alhabeb, M.; Maleski, K.; Anasori, B.; Lelyukh, P.; Clark, L.; Sin, S.; Gogotsi, Y. Guidelines for Synthesis and Processing of Two-Dimensional Titanium Carbide (Ti3C2Tx MXene). *Chem. Mater.* **2017**, *29*, 7633−7644.

(35) Ghidiu, M.; Lukatskaya, M. R.; Zhao, M. Q.; Gogotsi, Y.; Barsoum, M. W. Conductive two-dimensional titanium carbide 'clay' with high volumetric capacitance. *Nature* **2014**, *516*, 78−81.
(36) Al-Sehemi, A. G.; Irfan, A.; Asiri, A. M.; Ammar, Y. A. Synthesis, characterization and density functional theory study of low cost hydrazone sensitizers. *Bull. Chem. Soc. Ethiop.* **2015**, *29*, 137−148.
(37) Chen, L.; Bai, Z.; Zhu, L.; Zhang, L.; Cai, Y.; Li, Y.; Liu, W.; Wang, Y.; Chen, L.; Diwu, J.; Wang, J.; Chai, Z.; Wang, S. Ultrafast and Efficient Extraction of Uranium from Seawater Using an Amidoxime Appended Metal-Organic Framework. *ACS Appl. Mater. Interfaces* **2017**, *9*, 32446−32451.
(38) Ma, C.; Gao, J.; Wang, D.; Yuan, Y.; Wen, J.; Yan, B.; Zhao, S.; Zhao, X.; Sun, Y.; Wang, X.; Wang, N. Sunlight Polymerization of Poly(amidoxime) Hydrogel Membrane for Enhanced Uranium Extraction from Seawater. *Adv. Sci.* **2019**, *6*, 1900085.
(39) Fang, Y.; Liu, Z.; Han, J.; Jin, Z.; Han, Y.; Wang, F.; Niu, Y.; Wu, Y.; Xu, Y. High-Performance Electrocatalytic Conversion of N2 to NH3 Using Oxygen-Vacancy-Rich TiO2 In Situ Grown on Ti3C2Tx MXene. *Adv. Energy Mater.* **2019**, *9*, 1803406.
(40) Yang, S.; Lin, Y.; Song, X.; Zhang, P.; Gao, L. Covalently Coupled Ultrafine H-TiO2 Nanocrystals/Nitrogen-Doped Graphene Hybrid Materials for High-Performance Supercapacitor. *ACS Appl. Mater. Interfaces* **2015**, *7*, 17884−17892.
(41) Darabi, H. R.; Jafar Tehrani, M.; Aghapoor, K.; Mohsenzadeh, F.; Malekfar, R. A new protocol for the carboxylic acid sidewall functionalization of single-walled carbon nanotubes. *Appl. Surf. Sci.* **2012**, *258*, 8953−8958.
(42) Mesnage, A.; Lefevre, X.; Jegou, P.; Deniau, G.; Palacin, S. Spontaneous grafting of diazonium salts: chemical mechanism on metallic surfaces. *Langmuir* **2012**, *28*, 11767−11778.
(43) Yuan, Y.; Zhao, S.; Wen, J.; Wang, D.; Guo, X.; Xu, L.; Wang, X.; Wang, N. Rational Design of Porous Nanofiber Adsorbent by Blow-Spinning with Ultrahigh Uranium Recovery Capacity from Seawater. *Adv. Funct. Mater.* **2019**, *29*, 1805380.
(44) Chae, Y.; Kim, S. J.; Cho, S. Y.; Choi, J.; Maleski, K.; Lee, B. J.; Jung, H. T.; Gogotsi, Y.; Lee, Y.; Ahn, C. W. An investigation into the factors governing the oxidation of two-dimensional Ti3C2MXene. *Nanoscale* **2019**, *11*, 8387−8393.
(45) Ahmed, B.; Anjum, D. H.; Hedhili, M. N.; Gogotsi, Y.; Alshareef, H. N. H2O2 assisted room temperature oxidation of Ti2C MXene for Li-ion battery anodes. *Nanoscale* **2016**, *8*, 7580−7587.
(46) Ghassemi, H.; Harlow, W.; Mashtalir, O.; Beidaghi, M.; Lukatskaya, M. R.; Gogotsi, Y.; Taheri, M. L. In situ environmental transmission electron microscopy study of oxidation of two-dimensional Ti3C2and formation of carbon-supported TiO2. *J. Mater. Chem. A* **2014**, *2*, 14339−14343.
(47) Deysher, G.; Sin, S.; Gogotsi, Y.; Anasori, B. Oxidized 2D titanium carbide MXene. *Mater. Today* **2018**, *21*, 1064−1065.
(48) Sun, Y.; Wu, Z. Y.; Wang, X.; Ding, C.; Cheng, W.; Yu, S. H.; Wang, X. Macroscopic and Microscopic Investigation of U(VI) and Eu(III) Adsorption on Carbonaceous Nanofibers. *Environ. Sci. Technol.* **2016**, *50*, 4459−4467.
(49) He, Y.-R.; Li, S.-C.; Li, X.-L.; Yang, Y.; Tang, A.-M.; Du, L.; Tan, Z.-Y.; Zhang, D.; Chen, H.-B. Graphene (rGO) hydrogel: A promising material for facile removal of uranium from aqueous solution. *Chem. Eng. J.* **2018**, *338*, 333−340.
(50) Zhao, Y.; Li, J.; Zhang, S.; Wang, X. Amidoxime-functionalized magnetic mesoporous silica for selective sorption of U(vi). *RSC Adv.* **2014**, *4*, 32710−32717.
(51) Konstantinou, M.; Pashalidis, I. Competitive sorption of Cu(II), Eu(III) and U(VI) ions on TiO2 in aqueous solutions—A potentiometric study. *Colloids Surf., A* **2008**, *324*, 217−221.
(52) Ma, S.; Huang, L.; Ma, L.; Shim, Y.; Islam, S. M.; Wang, P.; Zhao, L. D.; Wang, S.; Sun, G.; Yang, X.; Kanatzidis, M. G. Efficient uranium capture by polysulfide/layered double hydroxide composites. *J. Am. Chem. Soc.* **2015**, *137*, 3670−3677.
(53) Wang, D.; Song, J.; Wen, J.; Yuan, Y.; Liu, Z.; Lin, S.; Wang, H.; Wang, H.; Zhao, S.; Zhao, X.; Fang, M.; Lei, M.; Li, B.; Wang, N.; Wang, X.; Wu, H. Significantly Enhanced Uranium Extraction from Seawater with Mass Produced Fully Amidoximated Nanofiber Adsorbent. *Adv. Energy Mater.* **2018**, *8*, 1802607.
(54) Manos, M. J.; Ding, N.; Kanatzidis, M. G. Layered metal sulfides: exceptionally selective agents for radioactive strontium removal. *Proc. Natl. Acad. Sci. U. S. A.* **2008**, *105*, 3696−3699.
(55) Zhao, G.; Jiang, L.; He, Y.; Li, J.; Dong, H.; Wang, X.; Hu, W. Sulfonated Graphene for Persistent Aromatic Pollutant Management. *Adv. Mater.* **2011**, *23*, 3959−3963.
(56) Ma, L.; Wang, Q.; Islam, S. M.; Liu, Y.; Ma, S.; Kanatzidis, M. G. Highly Selective and Efficient Removal of Heavy Metals by Layered Double Hydroxide Intercalated with the MoS42− Ion. *J. Am. Chem. Soc.* **2016**, *138*, 2858−2866.
(57) Huang, Z.; Li, Z.; Zheng, L.; Zhou, L.; Chai, Z.; Wang, X.; Shi, W. Interaction mechanism of uranium(VI) with three-dimensional graphene oxide-chitosan composite: Insights from batch experiments, IR, XPS, and EXAFS spectroscopy. *Chem. Eng. J.* **2017**, *328*, 1066−1074.
(58) Zhang, N.; Yuan, L. Y.; Guo, W. L.; Luo, S. Z.; Chai, Z. F.; Shi, W. Q. Extending the Use of Highly Porous and Functionalized MOFs to Th(IV) Capture. *ACS Appl. Mater. Interfaces* **2017**, *9*, 25216−25224.
(59) Porada, S.; Borchardt, L.; Oschatz, M.; Bryjak, M.; Atchison, J. S.; Keesman, K. J.; Kaskel, S.; Biesheuvel, P. M.; Presser, V. Direct prediction of the desalination performance of porous carbon electrodes for capacitive deionization. *Energy Environ. Sci.* **2013**, *6*, 3700−3712.
(60) Kim, J.; Choi, M. S.; Shin, K. H.; Kota, M.; Kang, Y.; Lee, S.; Lee, J. Y.; Park, H. S. Rational Design of Carbon Nanomaterials for Electrochemical Sodium Storage and Capture. *Adv. Mater.* **2019**, *31*, 1803444.
(61) Yin, H.; Zhao, S.; Wan, J.; Tang, H.; Chang, L.; He, L.; Zhao, H.; Gao, Y.; Tang, Z. Three-dimensional graphene/metal oxide nanoparticle hybrids for high-performance capacitive deionization of saline water. *Adv. Mater.* **2013**, *25*, 6270−6276.
(62) Tian, G.; Teat, S. J.; Zhang, Z.; Rao, L. Sequestering uranium from seawater: binding strength and modes of uranyl complexes with glutarimidedioxime. *Dalton Trans.* **2012**, *41*, 11579−11586.
(63) Abney, C. W.; Mayes, R. T.; Piechowicz, M.; Lin, Z.; Bryantsev, V. S.; Veith, G. M.; Dai, S.; Lin, W. XAFS investigation of polyamidoxime-bound uranyl contests the paradigm from small molecule studies. *Energy Environ. Sci.* **2016**, *9*, 448−453.